

XMM-NEWTON AND OPTICAL FOLLOW-UP OBSERVATIONS OF SDSS J093249.57+472523.0 AND
SDSS J102347.67+003841.2^{†,*}LEE HOMER¹, PAULA SZKODY¹, BING CHEN^{2,3}, ARNE HENDEN^{4,5,6}, GARY SCHMIDT⁷, SCOTT F. ANDERSON¹, NICOLE M. SILVESTRI¹ AND J. BRINKMANN⁸*Accepted for publication in the Astronomical Journal 2005 September 23*

ABSTRACT

We report follow-up *XMM-Newton* and ground-based optical observations of the unusual X-ray binary SDSS J102347.67+003841.2 (=FIRST J102347.6+003841), and a new candidate intermediate polar found in the Sloan Digital Sky Survey: SDSS J093249.57+472523.0. SDSS J1023 was observed in its low-state, with similar magnitude/color ($V = 17.4$ and $B = 17.9$), and smooth orbital modulation as seen in most previous observations. We further refine the ephemeris (for photometric minimum) to: $HJD(TT)_{\min} = 2453081.8546(3) + E * 0.198094(1)d$. It is easily detected in X-rays at an unabsorbed flux (0.01–10.0 keV) of $5 \times 10^{-13} \text{ erg cm}^{-2} \text{ s}^{-1}$. Fitting a variety of models we find that: (i) either a hot ($kT \gtrsim 15$ keV) optically thin plasma emission model (bremsstrahlung or MEKAL) or a simple power law can provide adequate fits to the data; (ii) these models prefer a low column density $\sim 10^{19} \text{ cm}^{-2}$; (iii) a neutron star atmosphere plus power law model (as found for quiescent low-mass X-ray binaries) can also produce a good fit (for plausible distances), though only for a much higher column $\approx 4 \times 10^{20} \text{ cm}^{-2}$ and a very cool atmosphere ($kT \lesssim 50$ eV). These results support the case that SDSS J1023 is a transient LMXB, and indeed places it in the subclass of such systems whose quiescent X-ray emission is dominated by a hard power law component. Our optical photometry of SDSS J0932 reveals that it is an high inclination eclipsing system. From our two epochs of data, and 7 eclipse times, we are able to derive a best fit ephemeris for minimum light: $HJD(TT)_{\min} = 2453122.2324(1) + E * 0.0661618(4)d$, although aliases, with one cycle count different between epochs, are acceptable. The X-ray spectrum is well fit by either a hard bremsstrahlung or power law, with a partial covering absorption model, with a high covering fraction ~ 0.9 and column $\approx 10^{23} \text{ cm}^{-2}$. Combined with its optical characteristics — high excitation emission lines, and brightness, yielding a large F_X/F_{opt} ratio — this highly absorbed X-ray spectrum argues that SDSS J0932 is a strong IP candidate. However, only more extensive optical photometry and a detection of its spin or spin-orbit beat frequency can confirm this classification.

Subject headings: individual: (SDSS J093249.57+472523.0, SDSS J102347.67+003841.2) — novae, cataclysmic variables — stars: magnetic — X-rays: stars

1. INTRODUCTION

Cataclysmic variables (CVs) and low-mass X-ray binaries (LMXBs) are two broad classes of interacting binary star, whose emission, from X-ray through optical/IR (and even radio), is powered by accretion onto a compact object (white dwarf or neutron star/black hole respectively). There are good reviews of the various subclasses and general characteristics in Warner (1995), and Lewin et al. (1995) respectively. When actively accreting, both classes exhibit (broad) emission line spectra, with very blue continua (from the accretion disk), but are normally distinguished by their relative X-ray output; their X-ray luminosity roughly scales as M_*/R_*^2 , i.e.

a factor of $10^4 - 10^5$. However, in many cases the accretion rate onto the compact object is highly variable, with both CVs and LMXBs exhibiting a variety of brightness states.

For the past three years, we have used *XMM-Newton* to study and confirm potential magnetic CVs identified in the Sloan Digital Sky Survey (York et al. 2000, SDSS). Two SDSS sources stood out based on the unusual strength of their He emission lines, as well as on the double-peaked character of all their lines. These are SDSS J102347.67+003841.2 (Szkody et al. 2003) and SDSS J093249.57+472523.0 (Szkody et al. 2004).

SDSS J102347.67+003841.2 = FIRST J102347.6+003841 (hereafter SDSS J1023) was identified as a CV, from its radio emission in the FIRST radio survey (Bond et al. 2002, , the first CV to be so discovered) , and independently from its color and emission line spectrum in the SDSS. In both cases, a highly magnetic white dwarf was suggested to account for the high-excitation optical emission lines and detectable radio emission. The nature of the lines appeared more consistent with an intermediate polar (IP), since they lacked both the large equivalent widths and narrow components usually seen in polars. Significant changes in state have been postulated to account for: (i) very different optical photometric behaviour seen by Bond et al. (2002) and later Woudt et al. (2004), a change from pure flickering behaviour to a smooth periodic modulation on a period of 4.75 hr; (ii) significant color changes between the SDSS photometry (when it appeared red) to the later SDSS spectroscopy, showing a very blue continuum.

[†] Some of the results presented here were obtained with the MMT Observatory, a facility operated jointly by The University of Arizona and the Smithsonian Institution.

^{*} Based on observations obtained with the Sloan Digital Sky Survey and with the Apache Point Observatory (APO) 3.5m telescope, which are owned and operated by the Astrophysical Research Consortium (ARC)

¹ Department of Astronomy, University of Washington, Box 351580, Seattle, WA 98195, USA

Electronic address: homer@astro.washington.edu

² XMM-Newton Science Operations Centre, ESA/Vilspa, 28080, Madrid, Spain

³ VEGA IT GmbH, c/o European Space Operations Centre, Darmstadt, Germany

⁴ Universities Space Research Association

⁵ US Naval Observatory, Flagstaff Station, P.O. Box 1149, Flagstaff, AZ 86002-1149, USA

⁶ American Association of Variable Star Observers, 25 Birch Street, Cambridge, MA 02138, USA

⁷ The University of Arizona, Steward Observatory, Tucson, AZ 85721, USA

spectroscopic campaign, which have called into question whether SDSS J1023 is a CV, or a LMXB instead. The low-state spectrum reveals a mid-G star, unlike either previous spectral observation. Multi-color photometry showed a smooth orbital modulation similar to Woudt et al. (2004), with color changes consistent with the changing aspect of the heated face of the secondary, but even at maximum light no emission lines are present in the spectrum. Modelling of the light curves, together with the radial velocity constraints, indicates that a high primary mass (greater than the Chandrasekhar mass) is needed, thus making SDSS J1023 a LMXB. We obtained X-ray, circular polarization and other optical data to further elucidate the nature of this source.

For SDSS J0932 we also obtained contemporaneous optical light curves, spectra and X-ray/optical data from *XMM-Newton* in an attempt to discern its nature and possible relation to SDSS J1023.

2. OBSERVATIONS

A summary of the X-ray and optical observations is presented in Table 1. *XMM-Newton* possesses three X-ray telescopes, backed by the two MOS and one pn (Turner et al. 2001) CCD cameras, and an optical monitor (OM, Strüder et al. 2001); hence parallel data are obtained by all detectors. The two Reflection Grating Spectrographs (den Herder et al. 2001) are arrayed in the optical path of the MOS detectors; however, for neither target were there sufficient counts to provide useful signal in the resulting dispersed spectra. In the direct (spectro)imaging EPIC detectors count rates were sufficient for extraction of low-resolution spectra and light curves. We followed the standard protocol as given by the Vilspa *XMM-Newton* Science Analysis System (SAS) site⁹ and the ABC guide¹⁰ from the US GOF. In both cases we used calibration files current to 2005 March 16 and the SAS v6.1.0, and as precaution we used SAS-tools to produce new event list files from the Observation Data Files incorporating the latest calibration updates.

To check on variations in the X-ray background we created light curves for each entire detector in the 10–15 keV range. No hard X-ray flaring events were present in the data, and for SDSS J1023 we simply used the standard good time intervals (GTIs). The case of SDSS J0932 was more complex. Due to its low count rate, the effects of background are relatively important. Examination of the background spectra showed the usual steep rise at low energies (due to detector noise) and a number of prominent metal lines, which are due to fluorescence of satellite materials bombarded by soft protons, especially in the pn. For the pn it is possible to make some improvements to reduce this detector background; we followed the guidelines in SAS handbook section 4.3.2.1 “Improving the quality of EPIC pn data: epreject.” Next, we created background light curves to examine any variations at these specific energies, and identified one interval of especially high flux, and created new GTIs to exclude it.

In addition to the time selection, we screened the event lists using the standard canned expressions and restricted energies to the 0.1–10 keV range. Owing to the very different count rates, we used different extraction radii for each source. For SDSS J0932 we used circular source apertures of radius 320 pixel (MOS) and 360 pixel (pn), in each case enclosing $\sim 70\%$ of the energy, chosen to maximize S/N. For SDSS J1023 we increased the radii to 480 and 640 pix respectively, now enclosing $\sim 80\%$ of the energy. For the background, we selected annuli on

the same chip for the MOS, and adjacent rectangular regions at similar detector Y locations to the target for the pn, excluding any point sources. As advised we selected single to quadruple events for the MOS (pattern ≤ 12), but only singles from the pn (pattern = 0).

Using the same extraction regions for source and background we extracted their light curves with SAS task `evselect`. In this instance (to maximise counts) we included both singles and doubles from the pn (pattern ≤ 4). Finally, background subtraction (scaled by extraction area) and correction of the time stamps to the heliocenter (times in HJD(TT)¹¹) were undertaken with `FTOOLS`¹². We obtained simultaneous *B*-band light curves from the OM. Again, we performed our own extractions using `omfchain` starting from the ODF event list files, setting our binning times at this earliest stage. We converted the count rates into magnitudes according to the results from interactive photometry with the `omsource` task.

SDSS J0932 was also observed by the US Naval Observatory Flagstaff Station (NOFS) 1m telescope on 2005 April 11 and May 12. The latter observation covers the 3 hr window immediately preceding the *XMM-Newton* observation (and OM optical coverage). To maximise signal-to-noise these data were taken in white light, but an approximate zeropoint for this differential photometry to Johnson $\sim V$ -band was made possible through calibration of the field from all-sky photometry including Landolt standards observed at NOFS. Hence, the light curves are labelled *V* magnitudes. A night after its X-ray observations (2005 May 13) a similar time series was taken on SDSS J1023. Circular spectropolarimetry and spectrophotometry was also obtained for SDSS J1023 with the CCD Spectropolarimeter SPOL (Schmidt et al. 1992) in 2002 May on the 2.3 m Kitt Peak Bok telescope and on the 6.5 m MMT in 2004 February, as indicated in Table 1. At both epochs, the object displayed the spectrum of a G star, with apparent magnitudes of 17.9 and 17.5, respectively. The 20 min observation sequences revealed no significantly polarized features, and respective upper limits are $v = V/I = 0.5\%$ and 0.03% when summed over the spectrum.

We also observed both SDSS J0932 and SDSS J1023 on 2005 May 23 with the double-imaging spectrograph (DIS) with a resolution of about 2Å on the Apache Point Observatory (APO) 3.5m (see fig. 1). These spectra were reduced and flux-calibrated using standard `IRAF`¹³ routines.

3. SDSS J1023

3.1. Light Curves

Figure 2 shows that when we combine our two optical light curves (phase-folded according to our refined ephemeris), we have full phase coverage. Again we see the same kind of smooth (but non-sinusoidal) modulation as observed by both Woudt et al. (2004) and TA05. Both our optical curves indicate a broad (~ 0.3 in phase) constant flux interval at maximum light, followed by a smooth rounded minimum. Excellent agreement is seen for the phasing of minimum light (posited as superior conjunction of the donor); 574 cycles have elapsed be-

¹¹ The tools actually yield barycentric Julian Date in the barycentric dynamical time system, BJD(TB). However, the offset to heliocentric Julian Date in the geocentric (terrestrial) dynamical time system (HJD(TT)) is less than ~ 3 s at any given time, fine for our purposes here.

¹² <http://heasarc.gsfc.nasa.gov/lheasoft/ftools/>

¹³ `IRAF` (Image Reduction and Analysis Facility) is distributed by the National Optical Astronomy Observatories, which are oper-

TABLE 1
OBSERVATION SUMMARY

SDSS J	UT Date	Obs	UT Time	Characteristics ^a	Comments
1023	2002 May 11	Bok:SPOL	03:54 - 04:17	circ. pol.< 0.5%	spectropolarimetry, 1200s
	2004 Feb 16	MMT:SPOL	08:40 - 09:02	circ. pol.< 0.03%	spectropolarimetry, 1200s
	2004 May 12	<i>XMM-Newton:</i>			
		EPIC-pn	10:44 - 14:37	0.08 cts s ⁻¹	12570s live time ^b
		EPIC-MOS1/2	10:21 - 14:42	0.03 cts s ⁻¹	15430s live time
		OM	10:30 - 14:14	<i>B</i> = 17.9	12899s duration
	2004 May 13	NOFS	03:12 - 06:55	~ <i>V</i> = 17.3 - 17.6	open filter photometry
	2004 May 23	APO: DIS	05:40 - 06:05	—	spectrum (poor fluxing)
	2004 Apr 11	NOFS	03:53 - 08:48	~ <i>V</i> = 18.5 - 19.0	open filter photometry
	2004 May 12	NOFS	03:08 - 06:41	~ <i>V</i> = 18.5 - 19.2	open filter photometry
	2004 May 12	<i>XMM-Newton:</i>			
		EPIC-pn	07:08 - 08:57	0.008 cts s ⁻¹	5698s live time
		EPIC-MOS1/2	06:46 - 02:00	0.003 cts s ⁻¹	7953/7984s live time
		OM	06:54 - 09:04	<i>B</i> = 19.1	7478s duration
	2004 May 23	APO: DIS	05:08 - 05:33	~ <i>V</i> = 19.3	spectrum

^aThe open filter photometry from NOFS has an estimated equivalent *V* zero-point, while for spectra the flux density at $\sim 5500\text{\AA}$ is used. The *XMM-Newton* count rates are average values for each observation for a single detector.

^bThe live time of the X-ray CCD detectors refers to the sum of the good-time intervals, less any dead time. It is typically much less than the difference of observation start and stop times.

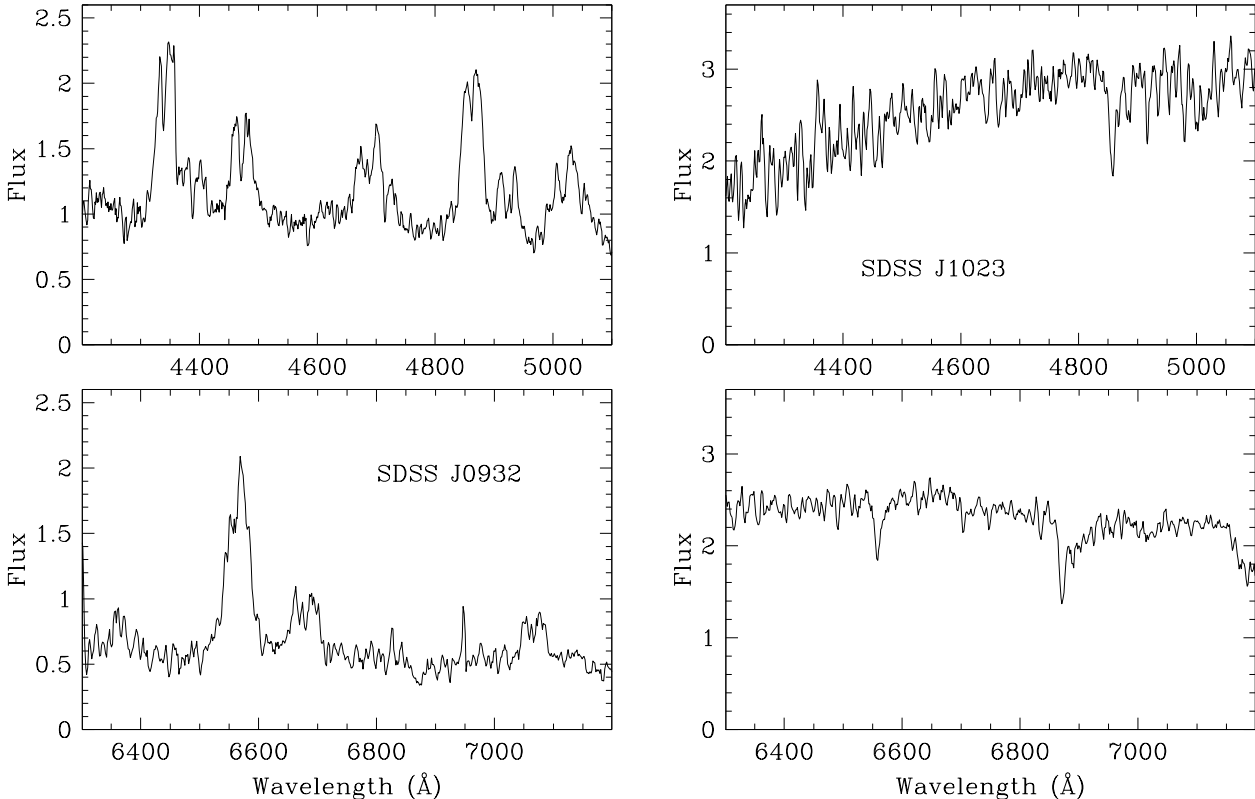


FIG. 1.— APO spectra of SDSS J0932 (left panels) and SDSS J1023 (right panels). SDSS J0932 was observed in a similar state to that seen during its SDSS spectroscopy; it exhibits strong He lines indicative of high-ionization states seen in magnetic CVs. In contrast, SDSS J1023 was observed in its low state, showing neither blue light from an accretion disc nor any emission lines. The flux scale is in units of flux density $10^{-16} \text{ erg cm}^{-2} \text{ s}^{-1} \text{ \AA}^{-1}$.

tween the TA05 ephemeris and our epoch of observation, giving a phase uncertainty of merely 0.006. Fitting a Gaussian to the minimum in the 2004 May 13 NOFS lightcurve we determine $T'_0 = 2453138.7077(3)$, giving $P' = \Delta(T_0)/574 = 113.7062(6)/574 = 0.198094(1)\text{d}$, and a refined ephemeris of:

$$\text{HJD(TT)} = -2453081.8546(3) + E * 0.198094(1)\text{d}$$

+ 64.184s at the current epoch).

We constructed the X-ray light curve (Fig. 2) by summing the background-subtracted light curves from all three EPIC cameras, with 300s bins. The X-ray light curve does not show a similar smooth modulation, but instead is quite irregular. Indeed, the amplitude of its

¹³ We use Terrestrial Time throughout this paper, since it the

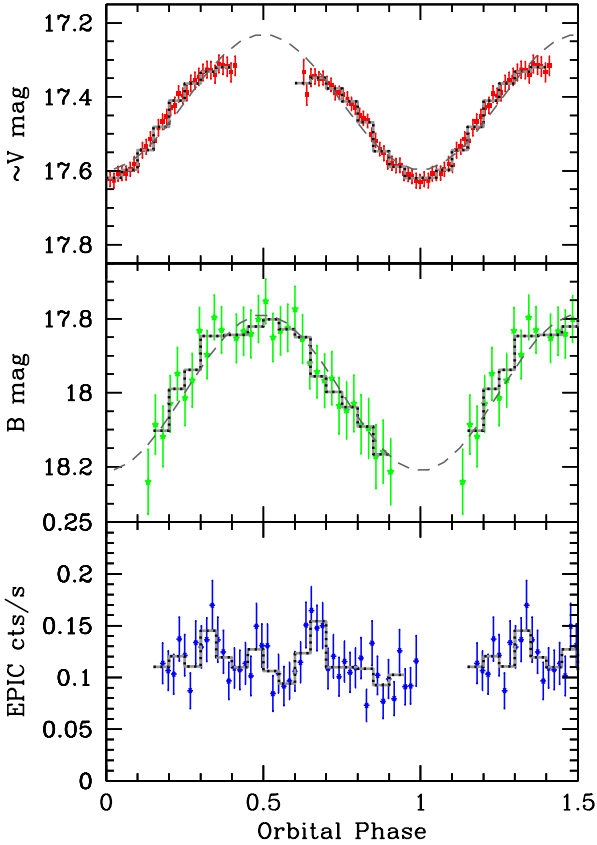


FIG. 2.— SDSS J1023: from top to bottom, light curves in white light from NOFS, B -band from the *XMM-Newton*/OM and in the X-ray (0.2–10 keV). They are plotted against phase according to our refined ephemeris. The optical curves show smooth, but non-sinusoidal profiles, as can be seen by the deviations from the overplotted best fit sinusoids.

variability (peak-peak) amounts to about 60%, greater than the 40% in B or 30% in white light. In view of the IP nature hypothesis, we note that it is possible to fit a sinusoid plus first harmonic model to our data, with a period of 0.069 ± 0.003 d (98 min), or $0.3 \times P_{\text{orb}}$. As to the significance of this signal, the peak in the Lomb-Scargle periodogram (Scargle 1982) is at the 96.5% confidence level, but we caution that with merely two cycles of coverage its reality remains debatable. Moreover, only three IPs have similarly large spin-orbit period ratios, V1025 Cen, DW Cnc and EX Hya, and all these are IPs below the period gap, with periods ~ 1.5 hrs. If this putative spin period were to be confirmed, it would place SDSS J1023 in a unique position in the $P_{\text{orb}} - P_{\text{spin}}$ diagram.

3.2. X-ray Spectral Fitting

Following the most recent guidelines on the low-energy EPIC calibrations, we restricted our fitting to > 0.2 keV for the MOS and > 0.15 keV for the pn, whilst still taking care to check the effects of different choices of these limits. After initial inspection of the data, showing a high energy tail, we used all good data below 15 keV for this relatively bright source. There were sufficient counts to bin the data at > 20 counts/bin, and use χ^2 statistics to find the best fits to the background subtracted source spectra. We also double-checked our results using > 5 counts/bin, and fitting simultaneous source and background spectra using Cash statistics; in all cases the

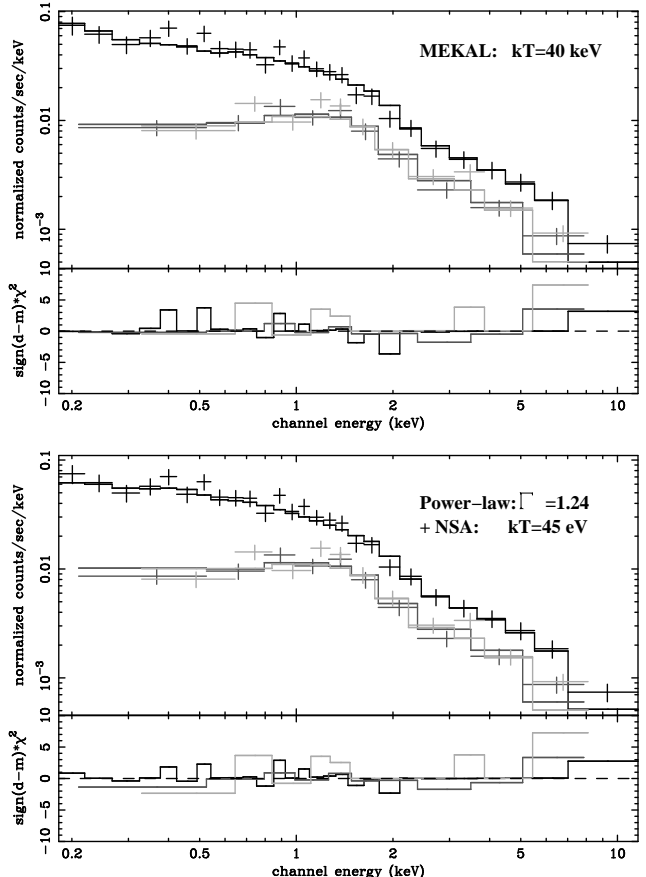


FIG. 3.— *XMM-Newton*/EPIC spectra for SDSS J1023: black–pn; dark grey–MOS1; light grey–MOS2. *Top*: best fit “CV” model consisting of a single temperature optically thin plasma model (MEKAL), absorbed by $N_H = 1 \times 10^{19}$ cm $^{-2}$. *Bottom*: best fit “quiescent LMXB” model comprising a soft neutron star atmosphere (NSA) and a simple power law, with a higher column of $N_H = 4.3 \times 10^{20}$ cm $^{-2}$.

simple single component plus interstellar absorbing column (see Table 2). In general the emission of CVs can be approximated with a thermal plasma. We performed fits setting $N_H = 4.22 \times 10^{20}$ cm $^{-2}$, the maximum Galactic column as derived from dust maps (using HEAsoft tool nH) or a fiducial $N_H = 1 \times 10^{19}$ cm $^{-2}$, appropriate for such a high Galactic latitude source, and lastly with this parameter free. A high temperature ($\gtrsim 30$ keV) thermal plasma (either bremsstrahlung, or bremsstrahlung plus lines– MEKAL) can produce an acceptable fit (see fig. 3) but only with the lower column option (leaving the column free yielded only an upper limit of $N_H = 4.4 \times 10^{19}$ cm $^{-2}$, but was consistent with zero). The best fit was a simple power law with $\chi^2_{\nu} \approx 1.0$ for either fixed column, and photon index of 1.3–1.5 (also see fig. 3). In this case, the data could roughly constrain the column, when freed, to $N_H = 9 \pm 7 \times 10^{19}$ cm $^{-2}$. A power law fit is suggestive of that found for the hard component of LMXBs in quiescence (see e.g. Campana et al. 1998).

Moving onto more complex models, we examined two temperature and multi-temperature MEKAL (XSPEC:CEMEKL) models–used to fit IP spectra, and lastly a soft blackbody + MEKAL as for a polar. A two temperature fit was possible, but in the case of the low column the higher temperature MEKAL pegged at its upper limit of 80 keV, whilst the cool plasma settled at 100–300 eV. The data were not suitable to constrain the CEMEKL model at all. Adding in a soft blackbody to a MEKAL fit has a similar effect as the two-temperature

TABLE 2
X-RAY SPECTRAL FITS FOR SDSS J1023

Model	reduced χ^2	$N_H \times 10^{20} \text{ cm}^{-2}$	kT^a (eV)	kT or Γ (keV)	Flux ^b
bremss	1.45	4.22 ^c	...	15^{+4}_{-2}	4.9 ± 0.4
	1.06	0.1	...	63^{+26}_{-30}	5.2 ± 0.8
MEKAL	1.38	4.22	...	12^{+3}_{-2}	5.1 ± 0.5
	1.02	0.1	...	39^{+24}_{-12}	5.1 ± 0.6
PL	1.16	4.22	...	1.47 ± 0.04	5.5 ± 0.3
	1.02	0.1	...	1.27 ± 0.03	5.3 ± 0.3
	1.02	0.9 ± 0.7	...	1.31 ± 0.05	5.3 ± 0.3
2 T MEKAL	1.09	4.22	98^{+6}_{-4}	23^{+14}_{-7}	11 ± 4
	0.99	0.1	300^{+24}_{-12}	$80^{+}\text{pegged}_{-35}$	$5.2^{+0.2}_{-0.4}$
BB + MEKAL	1.00	4.22	130 ± 20	$80^{+}\text{pegged}_{-42}$	5.5 ± 0.3
	0.98	0.1	220 ± 40	$80^{+}\text{pegged}_{-19}$	5.0 ± 0.3
PL + NSA:	1 kpc	1.02	4.22	33 ± 1	1.32 ± 0.05
		0.8 $^{+3.2}_{-0.7}$	< 21	$1.32^{+0.04}_{-0.05}$	6.0 ± 0.6
	2 kpc	1.00	4.22	45 ± 2	$1.27^{+0.05}_{-0.06}$
		1.01	$4.3^{+1.8}_{-2.1}$	45 ± 5	$1.24^{+0.07}_{-0.04}$
2.3 kpc	0.99	4.22	48 ± 2	$1.26^{+0.05}_{-0.06}$	5.8 ± 0.6
	1.02	$4.4^{+1.6}_{-1.4}$	48 ± 6	$1.32^{+0.06}_{-0.04}$	5.8 ± 0.6

^aFor neutron star atmosphere (NSA) model the effective temperature (for a distant observer) is quoted, i.e. $kT_{\text{eff}} = g_r \times T_{\text{eff}}$ where $g_r = (1 - 2.952 \times M_{\text{ns}}/R_{\text{ns}})^{0.5}$ is the gravitational redshift parameter.

^bUnabsorbed flux in the 0.01–10 keV range, in units of $10^{-13} \text{ erg cm}^{-2} \text{ s}^{-1}$.

^cModel parameters without quoted uncertainties have been fixed at the value given.

both cases $kT_{\text{MEKAL}} = 80 \text{ keV}$ (pegged). This compares to a typical polar fit with $\sim 30 \text{ eV}$ and 30 keV for these components.

On the other hand if SDSS J1023 is a LMXB, then we might expect a good fit for the typical two component neutron star atmosphere (NSA) plus power law model. Fixing both the neutron star radius and mass at their canonical 10 km and $1.4 M_{\odot}$ values, the only free parameters left in the NSA model are the distance and temperature. TA05 provide a constraint on the distance to SDSS J1023 depending on the mass of the secondary. We investigated fits for a range of masses/distances from $0.1 M_{\odot}$ (1.0 kpc) to $1.2 M_{\odot}$ (2.3 kpc). Statistically acceptable fits are found for all distances, although in all cases only for a higher column $\gtrsim 10^{20} \text{ cm}^{-2}$. However, especially for $d = 1 \text{ kpc}$, but also for the longer distances, the effective temperature of the NSA is low, and in all cases it contributes merely $\sim 10\%$ of the flux, even including energies down to 0.01 keV. If one performs an F -test to compare the best fit PL (which has a low column) to the best fit PL+NSA (which requires a higher column), the low value indicates that there is no need for the inclusion of the soft component to model the data; but of course this all depends on the actual column.

In general, the quality of the fits is fairly similar and each yields an unabsorbed 0.01–10 keV X-ray luminosity of $5 \times 10^{-13} \text{ erg cm}^{-2} \text{ s}^{-1}$. Although two-component models yield slightly better fits, in most cases consideration of the parameter values indicate problems: extreme plasma temperatures or unusually low/high temperatures for the neutron star (either NSA or blackbody). We defer further discussion to § 5.

4. SDSS J0932

4.1. Light Curves

Owing to the low X-ray count rate of this source it was

usefully be binned to 160s, similar to the time-resolution of the NOFS data. We present the three light curves from 2004 April and May in figure 4. Consistent with the double-peaked optical spectra, this source is clearly at a high-inclination to our line of sight, exhibiting deep, 2 magnitude eclipses. We have undertaken an $O - C$ analysis using the 7 eclipse times spanning roughly a month. From the 4 May points alone we can determine the period to within 0.2%. Unfortunately, this is not quite high enough precision to facilitate an unambiguous cycle count back to the April epoch. The best fit solution yields:

$$\text{HJD(TT)}_{\text{min}} = 2453122.2324(1) + E * 0.0661618(4) \text{ d.}$$

In table 3 and fig. 5 we present our full $O - C$ results for the 3 candidate solutions. Clearly, additional photometry will be needed to confirm the correct one.

SDSS J0932 exhibits variability in addition to its eclipses, which is notably different between the two epochs. In 2005 April there appears a long term trend, a slow rise and decline, with no obviously repeatable modulation on the orbital period. In contrast, in 2005 May, there is no long timescale change in flux, but there is a clear periodic smooth variation. Close inspection of the light curves in the lower panel of fig. 4 reveals a possible trend in the appearance of the pre-eclipse hump: it appears slightly later in phase each cycle. We fit a sinusoid plus first harmonic model to all the non-eclipse datapoints, this gives a best fit period of $0.0688^{+0.0012}_{-0.0006} \text{ d}$, which is 3.8% longer than the orbital period, hence nominally discrepant at the 4σ level. Again with merely four cycles of data, this period is far from conclusive. In fig. 6 we show the NOFS data folded on both the orbital period and this longer one. The obvious explanation for such a period a few percent longer than the orbital is

TABLE 3
OPTICAL ECLIPSE TIMINGS AND $O - C$ RESULTS FOR SDSS J0932.

HJD(TT) 2453000 +	$\sigma(\text{HJD})$ ($\times 10^{-4}$)	$P = 0.0663035(4)$ d		$P = 0.0661618(4)$ d		$P = 0.0660206(5)$ d	
		Cycle Count	$O - C$ (cycles $\times 10^{-5}$)	Cycle Count	$O - C$ (cycles $\times 10^{-5}$)	Cycle Count	$O - C$ (cycles $\times 10^{-5}$)
106.68445	4.5	1	3.3 ± 6.8	1	0.0 ± 6.8	1	-3.2 ± 6.8
106.75044	2.0	2	-1.4 ± 3.0	2	-2.5 ± 3.0	2	-3.7 ± 3.0
106.81690	2.8	3	1.0 ± 4.0	3	2.0 ± 4.2	3	3.0 ± 4.2
137.64816	1.6	468	2.9 ± 2.4	469	0.5 ± 2.4	470	-1.9 ± 2.4
137.71423	1.4	469	-0.5 ± 2.1	470	0.8 ± 2.1	471	-1.0 ± 2.1
137.78013	2.3	470	-6.6 ± 3.5	471	-4.7 ± 3.5	472	-2.8 ± 3.5
137.8470	3	471	1.4 ± 4.5	472	5.5 ± 4.5	473	9.6 ± 4.5

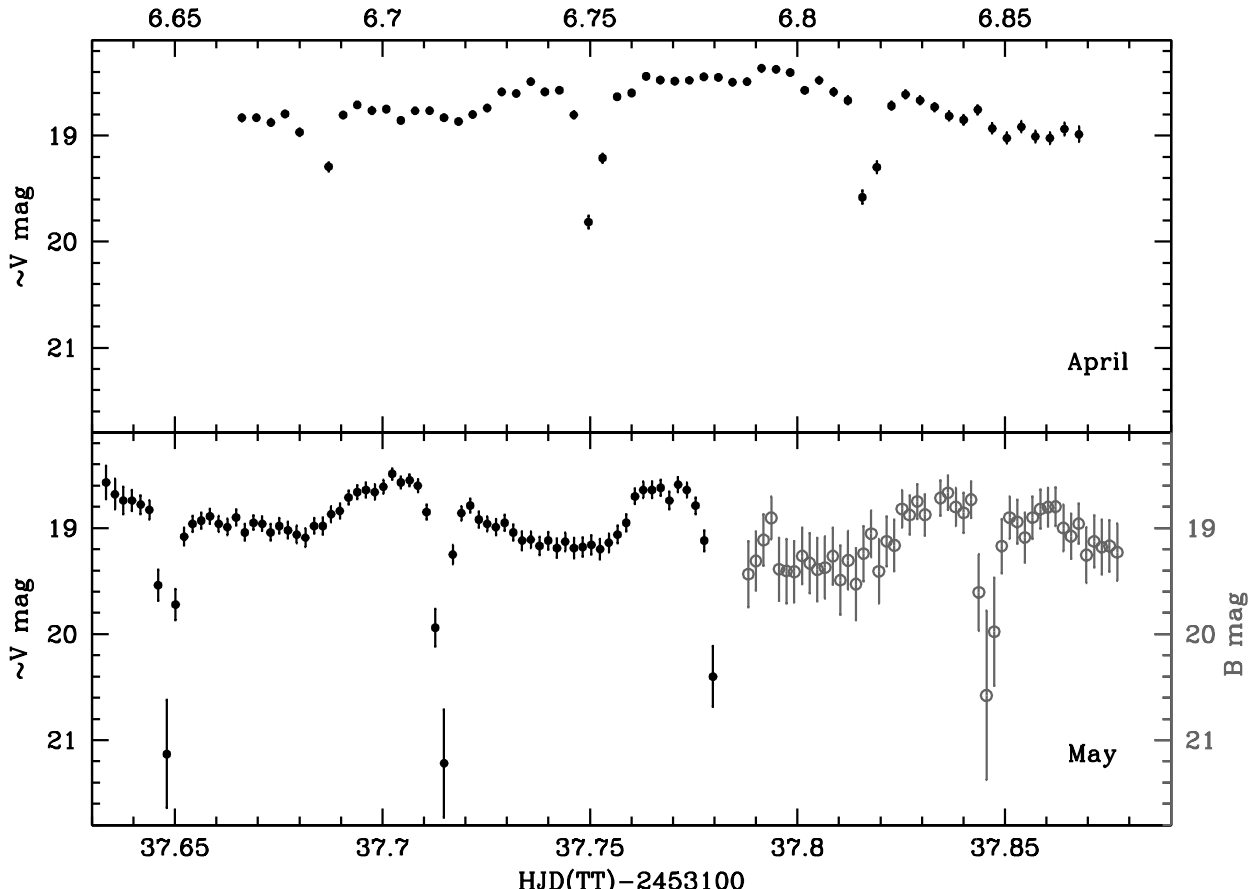


FIG. 4.— Optical light curves for SDSS J0932. Black filled circles (and error bars) show data from the NOFS 1-m telescope. These data were taken in white light; the $\sim V$ indicates that an approximate zero-pointing onto the Johnson system has been applied. Dark grey open circles show the B -band data from *XMM-Newton*/OM. Seven eclipses are clearly visible, as well as, non-eclipse modulation structure that changes significantly between the epochs.

4.2. X-ray Spectra

Even after our application of `epreject`, the background is estimated to contribute 45% of the pn flux within our source aperture (only $\lesssim 15\%$ for the MOS detectors). With 50 and 55 counts total in the pn and MOS detectors respectively, the use of smaller 5cts/bin binning and Cash statistics is the best approach. First, we examined and fit the background spectra. For this we could bin to 20cts/bin and still have good spectral resolution, and we simply aimed to find the best empirical model to represent these contributions. Our final model consists of a twice-broken power law (i.e. 3 different indices), plus Gaussian lines to account for the

Next, we used this model (with relative normalisations scaled according to extraction area) as the fixed background component in our source+background fitting.

With our poor statistics we concentrated on finding the simplest model fit to the data, starting with a bremsstrahlung plus a single absorption (i.e. for Galactic) column. First, we found that there is significant column in excess of that estimated for the line-of-sight, our best fit requiring $N_H = 5.6^{+2.0}_{-1.3} \times 10^{22} \text{ cm}^{-2}$, as compared to the dust-map estimate (from the `nH` tool) of $N_H = 1.39 \times 10^{20} \text{ cm}^{-2}$. Moreover, the temperature pegged at the 200 keV limit, well in excess of a physically plausible fit for a CV, indicating that this model is simply not able to fit the data.

TABLE 4
X-RAY SPECTRAL FITS FOR SDSS J0932

Model	Goodness of Fit	N_H (cm $^{-2}$)	N_H (cm $^{-2}$)	Partial covering frac.	kT (keV) or Γ	Flux ^b
bremss	70%	$6_{-1}^{+2} \times 10^{22}$	200 (pegged)	2.4 ± 0.8
	56%	$1.39_{-3}^{+5} \times 10^{20}$	$10_{-3}^{+5} \times 10^{22}$	0.95 ± 0.02	200 (pegged)	1.5 ± 0.7
	61%	1.39×10^{20}	$10_{-3}^{+5} \times 10^{22}$	0.95 ± 0.02	30	$1.5_{-0.3}^{+1.6}$
PL	76%	$3 \pm 3 \times 10^{22}$	0.5 ± 0.7	$_{-d}^{d}$
	59%	1.39×10^{20}	$9 \pm 5 \times 10^{22}$	0.9 ± 0.1	0.8 ± 0.6	1.7 ± 0.6

^aAs the fitting utilized Cash statistics, a Monte Carlo method was used to find the percentage of simulated spectra based on the parameter space of the model fit had C -statistic values less than than of the fit to the data. A good fit should have a value around 50%.

^bUnabsorbed flux in the 0.01–10 keV range, in units of 10^{-13} erg cm $^{-2}$ s $^{-1}$

^cModel parameters without quoted uncertainties have been fixed at the value given.

^dThe singly absorbed power law is such an unphysical fit that flux estimates were meaningless.

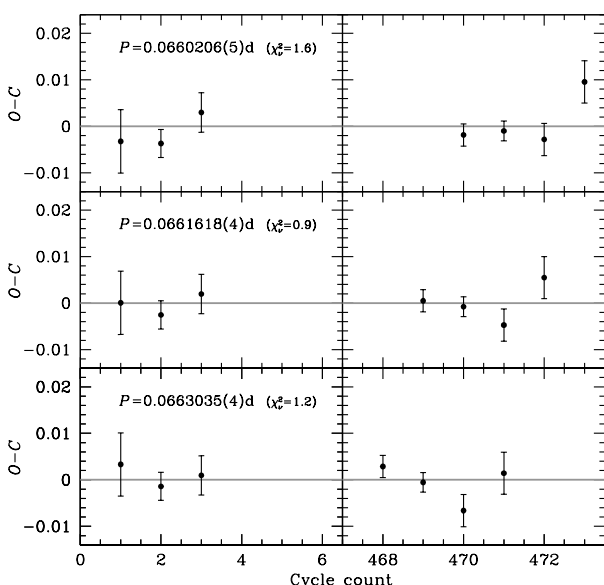


FIG. 5.— $O - C$ plots for the eclipse timings of SDSS J0932. The best fit is for $P = 0.0661618d$ but it is clear that a cycle count ambiguity of one between April and May observations makes little difference to the fits.

fit in this case gave $\Gamma = 0.5 \pm 0.7$ with $N_H = 3 \pm 3 \times 10^{22}$ cm $^{-2}$; generally poorly constrained and a poor goodness of fit of 76%¹⁴. For high-inclination LMXBs, it is often found that there is additional local absorption due to material vertically extended at the accretion disc rim (Church 2001), while for IPs the material in the accretion flow can have the same effect. In both cases, the absorption may only partially obscure the X-ray source spatially and, for the case of an orbitally averaged spectrum as we have here, only for part of an orbit. Hence, we included an additional column scaled by its partial covering fraction, whilst fixing the other at the nominal (maximum) Galactic value. The inclusion of this extra component does improve both fits, increasing the photon index, but the plasma temperature still pegs at its

¹⁴ This XSPEC command simulates a user defined number of spectra (we used 5000) based on the model and writes out the percentage of these simulations with the fit statistic less than that

maximum. At the same time, if we fix $kT_{br} = 30$ keV (typical for IPs) this only increases goodness from 56% to 61%. The covering fraction is in fact close to unity (0.9 ± 0.1 and 0.95 ± 0.02 respectively). In conclusion, our joint fits to the X-ray spectra (as shown in fig. 7, and detailed in Table. 4) can only constrain the absorption column, requiring a significant local absorption, which could equally be accounted for in a mCV interpretation or (high inclination) LMXB interpretation. As to the emission model, the data seem best fit with a power law, but this is far from conclusive.

5. NATURE OF SDSS J1023

The observational constraints supplied by our new optical and especially X-ray data lend significant support to the LMXB hypothesis of TA05. The 0.5–10 keV luminosity of SDSS J1023 is $10^{32.4}$ erg s $^{-1}$ assuming a distance of 2 kpc, which places it squarely in the range of luminosities for neutron star LMXBs in quiescence (see e.g. Campana & Stella 2004). However, in this energy range the flux is dominated (97%) by the hard power law component. Recently, Jonker et al. (2004b,a) examined the relation between the X-ray luminosity of neutron star transients in quiescence and the fractional contribution of the power law component. They found a correlation for $L_X \gtrsim 1 - 2 \times 10^{33}$ erg s $^{-1}$, and an anti-correlation for lower luminosities. With its relatively low luminosity SDSS J1023 lies at the top end of the anti-correlation having a negligible NSA contribution, similar to both the LMXB in Terzan 5 and the millisecond pulsar SAX J1808.4-3658 in quiescence. In the pulsar, the leading model for the power law component is the interaction of the pulsar wind with that from the donor star (Stella et al. 1994; Burderi et al. 2003), but as yet there is no clear origin for the case of weakly magnetized neutron stars. Since SDSS J1023 has not been observed with a large area X-ray detector, such as the *RXTE*, during an outburst, we have no constraints on its pulsed X-ray emission; it is interesting to speculate that it too may host a millisecond pulsar.

Another notable feature of SDSS J1023 is its short timescale (i.e. \sim 10's of minutes) X-ray variability; again this is somewhat unusual, but not without precedent, for example Cen X-4 and EXO 1745-248 (Campana et al. 2004; Wijnands et al. 2005). As for the spectral parameters themselves: with $kT_{eff} \approx 50$ eV it is lower than for most quiescent LMXBs (i.e. 100–300 eV), but fits in

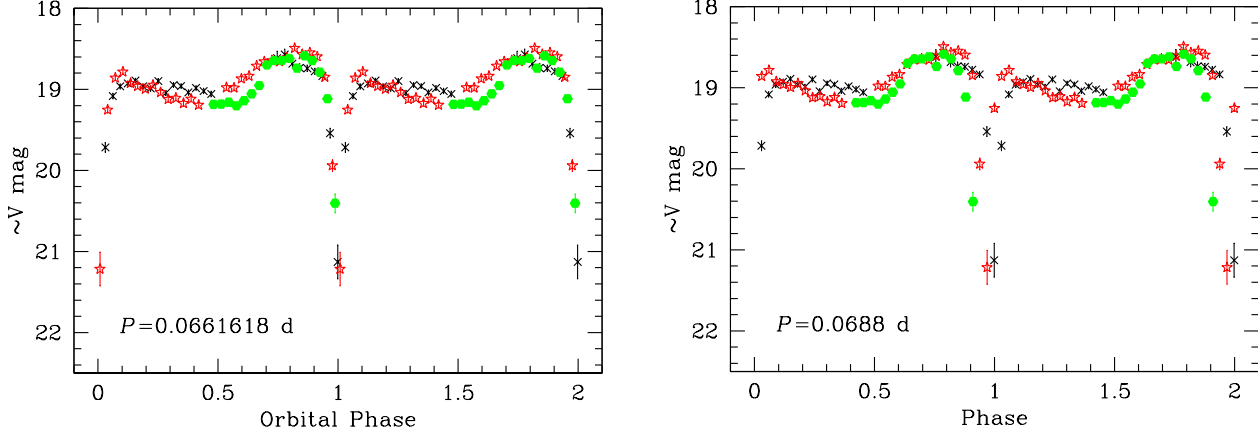


FIG. 6.— Optical light curves for SDSS J0932 from the 2005 May 13 observations. The data have been folded on: (left panel) the orbital period, as determined from eclipse timings; (right panel) a longer period of 0.0688 d, as given by a periodogram analysis of the out-of-eclipse modulation. Each cycle has been marked distinctly by different symbols (and colors- electronic edition only) to aid the eye.

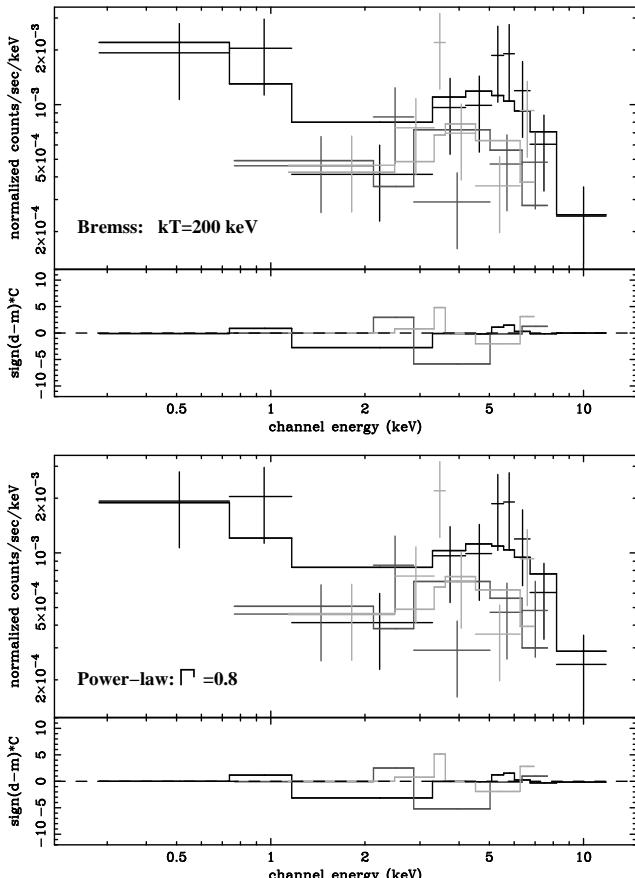


FIG. 7.— *XMM-Newton*/EPIC spectra for SDSS J0932: black—pn; dark grey—MOS1; light grey—MOS2. Top: best fit “CV” model consisting of a single temperature bremsstrahlung, with partial covering absorption (see text for details). Bottom: best fit “quiescent LMXB” – power law emission model instead.

normal 1–2 range.

Lastly, now that we have a measure of the quiescent X-ray luminosity, we can consider how much brighter it may have become during its active state (outburst), and consider its detectability during previous X-ray observations. A search of the HEASARC archives yields no previous pointed observations by other X-ray satellites. Naturally, its position was covered by both the *ROSAT* All-Sky Survey (RASS) and the *RXTE*/ASM, though in neither has

measures: we predict merely 0.015 counts/s in the RASS 0.5–2.5 keV band. However, the fact that SDSS J1023 remained undetected by the ASM even during its bright phase can provide a useful constraint. The nominal ASM point source sensitivity is 8.4×10^{-10} erg cm $^{-2}$ s $^{-1}$, hence SDSS J1023 could have brightened by a factor ~ 2000 and still remained undetected by the ASM. Such a brightening is well-within the wide spread seen amongst X-ray transients.

In addition to the X-ray, we can examine its activity history via a number of optical observations. Catalog data provide snapshots of its state at their epochs of observation. We have four independent data points spanning 1952 to 2000, and in each case the approximate *B* and *R* magnitudes show the source to be quiescent. Furthermore, all observations since the late 2000/early 2001 epoch of the Sloan spectroscopy and the Bond et al. series of observations show the source to be quiescent. It therefore appears that SDSS J1023 has a low-duty cycle of activity, which is seen in many other X-ray transients, and moreover, fits in with a low-temperature and luminosity from the neutron star atmosphere.

In summary, we can argue that all observations to date find a system with characteristics and behaviour fully consistent with a LMXB, which spends most of its time in quiescence.

For the CV alternative, we immediately run into problems: what provides its X-ray emission in such a quiescent state? A number of CVs are observed to enter very low states, optically up to ~ 7 mags fainter than normal: the VY Scl stars. However, they spend the majority of their time in active states. Only one IP has been observed to transition into such a very low-state, V1223 Sgr (Garnavich & Szkody 1988), in a survey of the Harvard plate collection, hence nothing more is known about its characteristics in that state. Physically, in the absence of mass transfer onto a white dwarf, the only plausible source of X-rays appears to be the chromospheric emission of the fast-rotating donor: as is the presumed case for SDSS J155331.12+551614.5 (Szkody et al. 2004). But for SDSS J1023, this option is inconsistent with the hardness of its X-ray spectrum. All active binaries when fit with optically thin thermal emission models yield temperature $\lesssim 2$ keV (see results from Chandra observations of 47 Tuc and from the RASS: Heinke et al. 2005; Dempsey et al. 1993), not $\gtrsim 15$ keV as we find. Moreover, the ratio of X-ray to optical flux

binaries.

6. NATURE OF SDSS J0932

Although the rough V magnitudes of SDSS J0932 (6 epochs- SDSS photometry through *XMM-Newton* observations) do vary, they differ by much less than a magnitude, which is likely due to random sampling of the eclipses in some of the longer exposures. With no clear evidence of significant state changes (unlike SDSS J1023) a transiently accreting LMXB (or dwarf nova) model seems less favored. In any case the high excitation lines of its optical spectra suggest either an active LMXB or magnetic CV. Furthermore, the high X-ray column (and partial covering model) further restrict the options to either a high-inclination LMXB or most likely an IP. As we noted, from the X-ray spectral fits alone it is hard to choose between these competing interpretations. Hence, we have also compared the X-ray to optical flux ratio of SDSS J0932 to those of all known IPs¹⁵ and to a sample of 8 high inclination LMXBs with periods less than 10 hrs. Clearly, the exact details of X-ray spectrum, and the Galactic absorption are not taken out in these estimates. Nevertheless, if we normalize our values such that SDSS J0932 has $F_X/F_{opt} = 1$ we find it fits well within the scatter of values for IPs, which range from 0.1 to 10, though clustered in the 1–2 range. In contrast, most of the high inclination (actively accreting) LMXBs have $F_X/F_{opt} \sim 100 – 1000$; low for LMXBs because the disk obscures much of the direct X-ray flux, but still orders of magnitude higher.

The absence of a firm detection of additional periodicities in the optical light curve leaves the IP candidacy of SDSS J0932 very much a matter of debate. There is also our tentative detection of a photometric variation a few percent longer than the orbital period, which would be difficult to explain in an IP. Much more extensive optical photometric monitoring is without doubt required to resolve these two issues.

7. CONCLUSIONS

We have obtained *XMM-Newton* X-ray and additional optical followup observations of two accreting binaries recently discovered in the SDSS: SDSS J1023 and SDSS J0932. Consideration of their optical spectra and magnitudes (and history thereof) suggests that we observed SDSS J1023 during its (normal) inactive state, while SDSS J0932 was actively accreting at the time.

¹⁵ See Koji Mukai's compendium, <http://lheawww.gsfc.nasa.gov/users/mukai/iphone/iphone.html>

For SDSS J1023 the X-ray results favor the (transient) LMXB hypothesis of Thorstensen & Armstrong (2005), both in terms of X-ray luminosity, spectral parameters and the relative contributions of the best fit neutron star atmosphere + power law model. The distance independent X-ray-to-optical flux ratio and the estimated range of X-ray luminosities are inconsistent with what we would expect from an inactive CV, i.e. the chromospheric emission from the low-mass donor star.

Our two epochs of time-series optical photometry confirm that SDSS J0932 is indeed a high inclination system, exhibiting deep eclipses on a period of 1.57 hr. Unfortunately, given the very low X-ray count rate of SDSS J0932 we are unable to construct a useful X-ray light curve. Neither are we able to constrain the emission model well but our X-ray spectra clearly require significant local absorption. This could be accounted for in either an Intermediate Polar or high inclination LMXB model. We find that its X-ray-to-optical flux is fully consistent with the known IPs, but at least an order of magnitude less than that of the X-ray faintest LMXB.

We thank the anonymous referee for their timely and helpful report. This work was supported by *XMM-Newton* grant NNG04GG66G to the University of Washington and is based on observations obtained with *XMM-Newton*, an ESA science mission with instruments and contributions directly funded by ESA Member States and the USA (NASA). G. Schmidt acknowledges the support of NSF grant AST 03-06080.

Funding for the creation and distribution of the SDSS Archive has been provided by the Alfred P. Sloan Foundation, the Participating Institutions, the National Aeronautics and Space Administration, the National Science Foundation, the U.S. Department of Energy, the Japanese Monbukagakusho, and the Max Planck Society. The SDSS Web site is <http://www.sdss.org/>.

The SDSS is managed by the Astrophysical Research Consortium (ARC) for the Participating Institutions. The Participating Institutions are The University of Chicago, Fermilab, the Institute for Advanced Study, the Japan Participation Group, The Johns Hopkins University, the Korean Scientist Group, Los Alamos National Laboratory, the Max-Planck-Institute for Astronomy (MPIA), the Max-Planck-Institute for Astrophysics (MPA), New Mexico State University, University of Pittsburgh, Princeton University, the United States Naval Observatory, and the University of Washington.

REFERENCES

Bond, H. E., White, R. L., Becker, R. H., & O'Brien, M. S. 2002, PASP, 114, 1359
 Burderi, L., Di Salvo, T., D'Antona, F., Robba, N. R., & Testa, V. 2003, A&A, 404, L43
 Campana, S., Colpi, M., Mereghetti, S., Stella, L., & Tavani, M. 1998, A&A Rev., 8, 279
 Campana, S., Israel, G. L., Stella, L., Gastaldello, F., & Mereghetti, S. 2004, ApJ, 601, 474
 Campana, S. & Stella, L. 2004, Nuclear Physics B Proceedings Supplements, 132, 427
 Church, M. J. 2001, Adv. Sp. Res., 28, 323
 Dempsey, R. C., Linsky, J. L., Schmitt, J. H. M. M., & Fleming, T. A. 1993, ApJ, 413, 333
 den Herder, J. W. et al. 2001, A&A, 365, L7
 Garnavich, P. & Szkody, P. 1988, PASP, 100, 1522
 Heinke, C. O., Grindlay, J. E., Edmonds, P. D., Cohn, H. N., Lugger, P. M., Camilo, F., Bogdanov, S., & Freire, P. C. 2005, ApJ, 625, 796
 Jonker, P. G., Galloway, D. K., McClintock, J. E., Buxton, M., Wijnands, R., Heinke, C. O., Pooley, D., Edmonds, P. D., Lewin, W. H. G., Grindlay, J. E., Jonker, P. G., & Miller, J. M. 2005, ApJ, 618, 883
 Woudt, P. A., Warner, B., & Pretorius, M. L. 2004, MNRAS, 351, 1015
 Lewin, W. H. G., van Paradijs, J., & Taam, R. E. 1995, in X-ray Binaries, ed. W. H. G. Lewin, J. van Paradijs, & E. P. J. van den Heuvel (Cambridge: Cambridge University Press), p. 175
 Patterson, J. 1998, PASP, 110, 1132
 Scargle, J. D. 1982, ApJ, 263, 835
 Stella, L., Campana, S., Colpi, M., Mereghetti, S., & Tavani, M. 1994, ApJ, 423, L47
 Strüder, L. et al. 2001, A&A, 365, L18
 Szkody, P. et al. 2003, AJ, 126, 1499
 —. 2004, AJ, 128, 1882
 Thorstensen, J. R. & Armstrong, E. 2005, AJ, 130, 759
 Turner, M. J. L. et al. 2001, A&A, 365, L27
 Warner, B. 1995, Cataclysmic Variable Stars (Cambridge University Press), 57

